Journal of ELECTRONIC MATERIALS, Vol. 45, No. 11, 2016
DOI: 10.1007/s11664-016-4809-6

Temperature-Dependent Electrical Properties and Carrier Transport Mechanisms of TMAH-Treated Ni/Au/Al_2O_3/GaN MIS Diode

M. SIVA PRATAP REDDY,[1,6] PEDDATHIMULA PUNEETHA,[2] V. RAJAGOPAL REDDY,[3] JUNG-HEE LEE,[4] SEONG-HOON JEONG,[1] and CHINHO PARK[5,7]

1.—Department of Electronic Engineering, LED-IT Fusion Technology and Research Center, Yeungnam University, Gyeongsan-si, Gyeongbuk 712-749, Korea. 2.—Department of Mechanical Engineering, Chadalawada Ramanamma Engineering College, Tirupati 517-506, India. 3.—Department of Physics, Sri Venkateswara University, Tirupati 517-502, India. 4.—School of Electrical Engineering and Computer Science, Kyungpook National University, Daegu 702-701, Korea. 5.—School of Chemical Engineering, Yeungnam University, Gyeongsan-si, Gyeongbuk 712-749, Korea. 6.—e-mail: drmspreddy@liftrc.re.kr. 7.—e-mail: chpark@ynu.ac.kr

The temperature-dependent electrical properties and carrier transport mechanisms of tetramethylammonium hydroxide (TMAH)-treated Ni/Au/Al_2O_3/GaN metal–insulator–semiconductor (MIS) diodes have been investigated by current–voltage (I–V) and capacitance–voltage (C–V) measurements. The experimental results reveal that the barrier height (I–V) increases whereas the ideality factor decreases with increasing temperature. The TMAH-treated Ni/Au/Al_2O_3/GaN MIS diode showed nonideal behaviors which indicate the presence of a nonuniform distribution of interface states (N_{SS}) and effect of series resistance (R_S). The obtained R_S and N_{SS} were found to decrease with increasing temperature. Furthermore, it was found that different transport mechanisms dominated in the TMAH-treated Ni/Au/Al_2O_3/GaN MIS diode. At 150 K to 250 K, Poole–Frenkel emission (PFE) was found to be responsible for the reverse leakage, while Schottky emission (SE) was the dominant mechanism at high electric fields in the temperature range from 300 K to 400 K. Feasible energy band diagrams and possible carrier transport mechanisms for the TMAH-treated Ni/Au/Al_2O_3/GaN MIS diode are discussed based on PFE and SE.

Key words: GaN MIS diodes, tetramethylammonium hydroxide, reverse leakage current, transport mechanisms, Poole–Frenkel emission, Schottky emission

INTRODUCTION

GaN-based optoelectronic and microelectronic devices have been rapidly developed due to their potential applications in the next-generation.[1–5] Remarkably, the GaN metal–insulator–semiconductor (MIS) diode is a workhorse of power electronics technology and a cornerstone for high-power, high-frequency, and high-temperature applications.[6–8] Fabrication of high-quality MIS diodes with low surface morphology and physical damage (caused by plasma etching) has considerable technological importance. Owing to the technological importance of MIS diodes, their electrical properties at room as well as cryogenic temperatures are significant.[9] Study of the I–V characteristics of such diodes at room temperature alone does not provide complete information about their carrier conduction process.[10,11] However, it is important to understand the carrier conduction process or nature of barrier

(Received January 16, 2016; accepted July 13, 2016; published online August 2, 2016)

formation at the semiconductor interface.[10,11] In particular, applications such as infrared detectors, sensors for thermal imaging, microwave diodes, and nuclear particle analysis detectors require knowledge about MIS diode characteristics based on temperature. The temperature-dependent characteristics allow identification of distinct conduction mechanism modes across MIS interfaces as well as study of the effects of parameters such as series resistance and interface state density on carrier transport at MIS interfaces.

Several researchers have explored the significance of the temperature-dependent characteristics of different insulator materials for GaN-based devices and explained the physical phenomenon of carrier transport mechanisms based on current–voltage (I–V) and capacitance–voltage (C–V) measurements.[11–15] Tekeli et al.[11] fabricated (Ni/Au)-$Al_{0.3}Ga_{0.7}N$/AlN/GaN heterostructures and studied their temperature-dependent inhomogeneous characteristics in the temperature range from 295 K to 415 K. The results revealed that the series resistance (R_S) exhibits unusual behavior, increasing with temperature. Lee et al.[12] studied a hydrogen sensor diode based on a β-Ga_2O_3 oxide layer obtained by the reactive oxidation method. They showed that the hydrogen sensing response of the Pt/β-Ga_2O_3/GaN diode decreased when operated at higher temperature. Lakshmi et al.[13] reported the temperature-dependent I–V and C–V characteristics of Au/SiO_2/n-GaN Schottky barrier diodes (SBDs) in the wide temperature range from 120 K to 390 K, and explained the results with the help of a double Gaussian distribution of barrier heights. Also, they showed that the interface state density decreased with an increase in temperature. Yang et al.[14] carried out frequency-dependent conductance measurements on AlGaN/GaN metal–oxide–semiconductor (MOS) structures with and without oxide (Al_2O_3) layer at room temperature. They demonstrated reduced trap density by eliminating the damage on the AlGaN/GaN surface by gate recession before Al_2O_3 deposition. Shetty et al.[15] fabricated a Pt/insulator layer (HfO_2)/n-GaN diode, reporting improved electrical characteristics compared with the Pt/n-GaN diode. They found that the barrier height (φ_{bo}^{IV}) increases while the ideality factor (n) decreases with increase in temperature.

For the present work, Al_2O_3 was selected as an insulator layer, because atomic layer deposited (ALD) Al_2O_3 has been explored as an insulator for GaN metal–oxide–semiconductor field-effect transistors (MOSFETs) and metal–oxide–semiconductor high-electron-mobility transistors (MOS-HEMTs), mainly due to its ability to form normally-off high-voltage power switching devices.[16–18] Generally, in MIS device fabrication, damage to the Schottky region due to plasma etching before Al_2O_3 deposition represents an obstacle to obtaining a high-quality insulating layer on a GaN surface. To address this issue, use of a chemical wet etching method could be a good solution. Indeed, anisotropic etching is a key technology for fabrication of various micromechanical devices. In particular, tetramethylammonium hydroxide (TMAH)-based wet etchant is believed to be an effective chemical solution in an anisotropic etching field.[19] Use of this type of wet etchant smoothens the roughened surface and also removes surface damage caused by plasma etching, being crucial for development of metal–semiconductor contacts. Our previous studies[20,21] firstly reported the effect of TMAH treatment as a post-gate-recess etching process for normally-off Al_2O_3/GaN MOSFETs, also revealing improved characteristics. They secondly reported improvement in the electrical characteristics of the Ni/Au/Al_2O_3/GaN MIS diode with application of simple TMAH treatment. Improved device performance was achieved when using TMAH treatment compared with diodes not treated using TMAH, indicating that TMAH treatment plays a positive role for effective removal of damage to the GaN surface due to plasma etching in the Schottky region. These features are quite interesting for fabrication of metal–insulator–GaN contacts based on TMAH wet etching. From the standpoint of TMAH treatment of devices, it is important to understand the effect of TMAH treatment on the temperature-dependent characteristics of MIS diodes. To the best of our knowledge, there are no reports on the temperature-dependent characteristics of MIS diodes after TMAH treatment.

Therefore, in this work, an attempt was made to investigate the electrical properties and carrier transport mechanisms of the TMAH-treated Ni/Au/Al_2O_3/GaN MIS diode in the temperature range from 150 K to 400 K in steps of 50 K based on current–voltage (I–V) and capacitance–voltage (C–V) measurements. The barrier height (ϕ_{bo}), ideality factor (n), series resistance (R_S), and interface state density (N_{SS}) of the TMAH-treated Ni/Au/Al_2O_3/GaN MIS diode were estimated as functions of temperature and discussed. In addition, the carrier transport mechanisms in Ni/Au/Al_2O_3/GaN MIS diodes as well as the dependence of the leakage current on the electric field at different temperatures are presented. The energy band diagrams and possible carrier transport mechanisms in the TMAH-treated Ni/Au/Al_2O_3/GaN MIS diode are also discussed based on the Poole–Frenkel and Schottky emission theories.

EXPERIMENTAL PROCEDURES

AlGaN/GaN epitaxial heterostructure was grown on sapphire substrates using a vertical-type metalorganic chemical vapor deposition (MOCVD) system with trimethylaluminum (TMAl), triethylgallium (TEGa), and ammonia (NH_3) as precursors and hydrogen as carrier gas. Prior to epitaxial heterostructure growth, the sapphire substrates were annealed at 1050°C for 10 min to

remove surface contamination. A 30-nm low-temperature GaN nucleation layer was grown at 500°C with chamber pressure of 5.3 kPa and V/III ratio of 2000. The low-temperature growth rate was controlled by flow of 27 μM/min TEGa and 0.09 M/min NH_3 precursors. Then, the susceptor temperature was ramped to 1020°C, and a 2-μm-thick undoped GaN semi-insulating layer was grown, followed by an AlGaN barrier layer (25 nm thick). The active region of the device was isolated by transformer-coupled plasma reactive-ion etching using BCl_3/Cl_2 gas mixture to fabricate the metal–insulator–semiconductor (MIS) device. The AlGaN layer in the Schottky region was fully recessed using the same gas mixture. To fabricate the TMAH-based MIS diode, the exposed GaN surface was treated with TMAH:H_2O (1:3) solution at 85°C for 10 min to smooth the surface and remove plasma damage. After TMAH treatment, a thin (3 nm) Al_2O_3 insulator layer was then deposited on the GaN surface by atomic layer deposition (ALD) at 450°C. Ohmic contacts were formed by a Ti/Al/Ni/Au (12 nm/200 nm/40 nm/100 nm) metal stack, annealed at 850°C using a rapid thermal annealing (RTA) system in N_2 ambient for 30 s. To complete device fabrication, Schottky contacts were formed on the TMAH-treated GaN surface by evaporating a Ni/Au (100 nm/120 nm) metal scheme at vacuum pressure of 6×10^{-4} Pa. The diameter of the Schottky diode was 500 μm. Current–voltage (I–V) and capacitance–voltage (C–V) characteristics were obtained using a precision semiconductor parameter analyzer (Agilent 4155C) and inductance (L), capacitance (C), and resistance (R) meter (Agilent 4248A).

RESULTS AND DISCUSSION

Figure 1 shows the forward and reverse current–voltage (I–V) characteristics of the TMAH-treated Ni/Au/Al_2O_3/GaN MIS diodes over the temperature range from 150 K to 400 K. A schematic diagram of the Ni/Au/Al_2O_3/GaN MIS diode is shown in the inset of Fig. 1. To obtain the barrier height and ideality factor (n), the forward-bias characteristics in terms of thermionic emission (TE) over the barrier were analyzed using the equation[22,23]

$$I = I_0 \exp\left(\frac{qV}{nk_BT}\right)\left[1 - \exp\left(\frac{-qV}{k_BT}\right)\right], \quad (1)$$

with

$$I_0 = AA_R^*T^2 \exp\left(\frac{-q\phi_{bo}^{IV}}{k_BT}\right), \quad (2)$$

where A is the contact area, T is absolute temperature, k_B is the Boltzmann constant, ϕ_{bo}^{IV} is the Schottky barrier height (SBH), and A_R^* is the modified Richardson constant, assumed to be 26.4 A/(cm K)^2 for n-type GaN. The ideality factor was obtained from the slope of the straight-line region of the forward-bias I–V characteristics. The

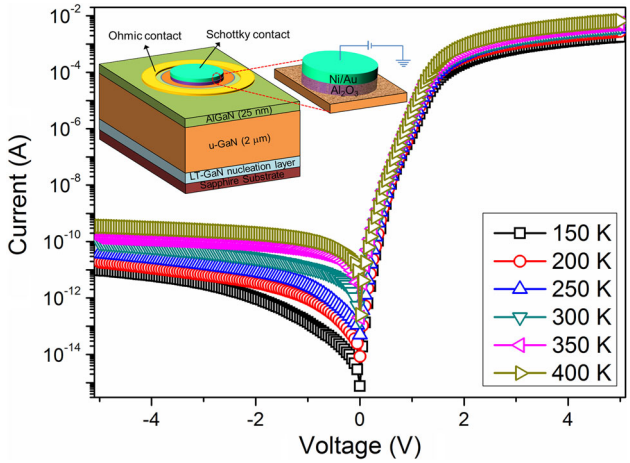

Fig. 1. Current–voltage curves of TMAH-treated Ni/Au/Al_2O_3/GaN MIS diode as function of temperature. Inset shows schematic configuration of TMAH-treated Ni/Au/Al_2O_3/GaN MIS diode.

diodes showed concrete manners with ideality factor of 2.98, 2.11, and 1.45 at 150 K, 200 K, and 250 K, respectively. However, note that the ideality factor improved with temperature to 1.12, 1.10, and 1.09 at 300 K, 350 K, and 400 K, respectively. The SBH for the diodes at 150 K, 200 K, 250 K, 300 K, 350 K, and 400 K was estimated to be 0.49 eV, 0.64 eV, 0.75 eV, 0.84 eV, 0.91 eV, and 0.96 eV, respectively. Clearly, as seen from Table I, the barrier height increases with temperature. As the temperature increases, more carriers have sufficient energy to overcome the higher barriers at the MIS interface. In addition, note that the ideality factor increased with decrease in temperature. For higher temperatures, the experimental ideality factor was almost equal to unity and was temperature dependent, which may be described as the "T_0 effect or anomaly."[22,24] These behaviors of the ideality factor have been attributed to inhomogeneities in the Schottky interface. As the temperature is decreased, the function current is dominated by low-Schottky-barrier regions with lower effective barriers and higher ideality factor.[24,25] Moreover, the ideality factor is not constant with temperature, showing linear behavior with inverse temperature. As a result, the ideality factor decreases with increasing temperature, whereas the barrier height increases. The TMAH-treated Ni/Au/Al_2O_3/GaN MIS diode showed nearly ideal behavior with ideality factor of 1.14 at 300 K. This value is comparable to the value reported by Lakshmi et al.[13] for Au/SiO_2/n-GaN diodes at 300 K. In this work, it was observed that TMAH treatment of the GaN diode decreased the ideality factor due to the influence of surface modification of the Al_2O_3/GaN interface. Note that the decrease in the ideality factor for the TMAH-treated Ni/Au/Al_2O_3/GaN MIS diode was achieved due to reduction of fabrication-induced defects at the MIS interface.[25] In addition, the applying-bias

Table I. Temperature-dependent parameters ϕ_{bo}, n, and R_S determined from I–V measurements in the temperature range from 150 K to 400 K for TMAH-treated Ni/Au/Al_2O_3/GaN MIS diode

Temperature (K)	ϕ_{bo} from I–V (eV)	n from I–V	n from dV/d(ln I)	ϕ_{bo} from $H(I)$ (eV)	R_S from dV/d(ln I) (Ω)	R_S from $H(I)$ (Ω)
150	0.49	2.98	3.01	0.47	1887.95	1854.92
200	0.64	2.11	2.14	0.62	1197.86	1180.77
250	0.75	1.45	1.48	0.73	954.38	948.25
300	0.84	1.12	1.14	0.82	693.04	688.57
350	0.91	1.10	1.12	0.89	571.24	568.41
400	0.96	1.09	1.10	0.94	475.03	470.64

dependence on the barrier height at the real MIS interfaces.[26]

The forward-bias I–V characteristics of the TMAH-treated Ni/Au/Al_2O_3/GaN MIS diode may deviate considerably from linearity due to the influence of the series resistance (R_S) and interface state density (N_{SS}) at sufficiently high voltages. Thus, it is important to understand the effect of R_S in the TMAH-treated Ni/Au/Al_2O_3/GaN MIS diode. To determine the R_S, ideality factor, and barrier height of the TMAH-treated Ni/Au/Al_2O_3/GaN MIS diode, Cheung's functions were applied. Cheung's functions can be expressed as[27]

$$\frac{dV}{d\ln I} = IR_S + n\frac{kT}{q}, \tag{3}$$

$$H(I) = V - n\frac{kT}{q}\ln\left(\frac{I}{AA^*T^2}\right), \tag{4a}$$

and

$$H(I) = n\phi_{bo} + IR_S. \tag{4b}$$

Figure 2 shows plots of dV/d(ln I) versus I and of $H(I)$ versus I for the Ni/Au/Al_2O_3/GaN MIS diode as a function of temperature. From Eq. 3, on a plot of dV/d(ln I) versus I (Fig. 2a), the y-axis intercept is nkT/q whereas the slope is R_S. Meanwhile, it is predicated that a linear curve fit to a plot of $H(I)$ versus I (Fig. 2b) will yield R_S from the slope and the barrier height from the ordinate, using the ideality factor obtained from Eq. 3 in Eq. 4a and b. Such calculations for Fig. 2a yielded R_S and n values of 1887.95 Ω and 3.01 at 150 K and 475.03 Ω and 1.10 at 400 K, respectively. Meanwhile, the values of R_S and barrier height obtained from Fig. 2b were 1854.92 Ω and 0.47 eV at 150 K and 470.64 Ω and 0.94 eV at 400 K, respectively, for the TMAH-treated Ni/Au/Al_2O_3/GaN MIS diode. It is clearly observed that the barrier heights obtained from Cheung's method are consistent with the values obtained by the I–V method. Also, the values of R_S obtained from the dV/d(ln I) versus I and $H(I)$ versus I plots are in good agreement at each temperature, as shown in Table I.

To characterize the interface quality of the MIS diode, C–V characteristics were determined.

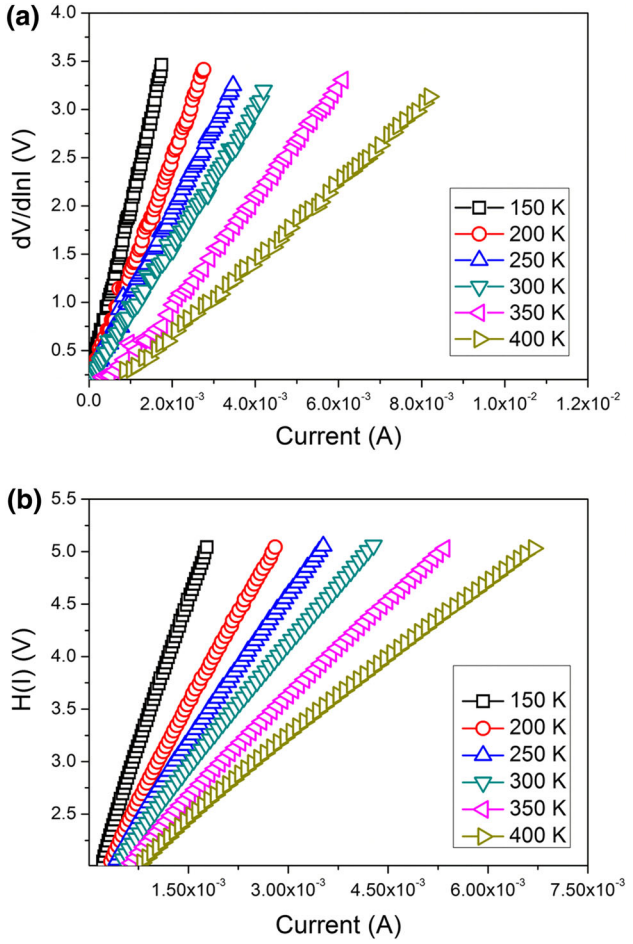

Fig. 2. Cheung plots of (a) dV/d(ln I) versus I and (b) $H(I)$ versus I for TMAH-treated Ni/Au/Al_2O_3/GaN MIS diode as function of temperature.

Figure 3 shows the forward- and reverse-bias C–V characteristics of the TMAH-treated Ni/Au/Al_2O_3/GaN MIS diode at different frequencies at room temperature (T = 300 K). It is clearly observed from Fig. 3 that the capacitance is high at low frequency (f = 10 kHz) but low at high frequencies (f = 100 kHz and 1 MHz). The capacitance is high at low frequencies because all the interface states are affected by the applied alternating-current (ac) signal and are able to give up and accept charges in

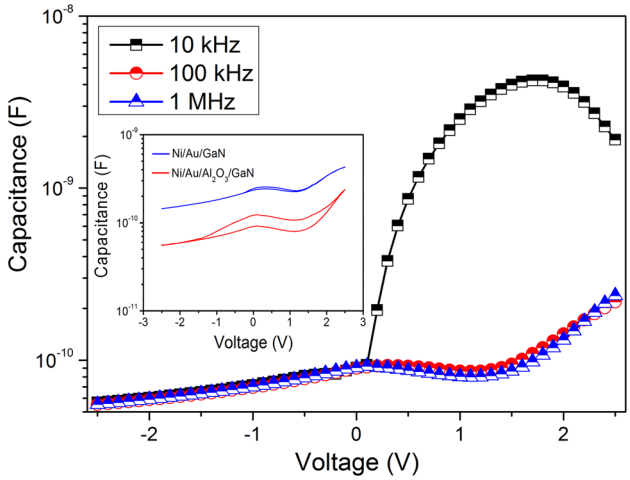

Fig. 3. *C–V* characteristics of TMAH-treated Ni/Au/Al_2O_3/GaN MIS diode at different frequencies at room temperature. Inset shows MOS *C–V* measurements of TMAH-treated Ni/Au/GaN and Ni/Au/Al_2O_3/GaN MIS diodes at 1 MHz.

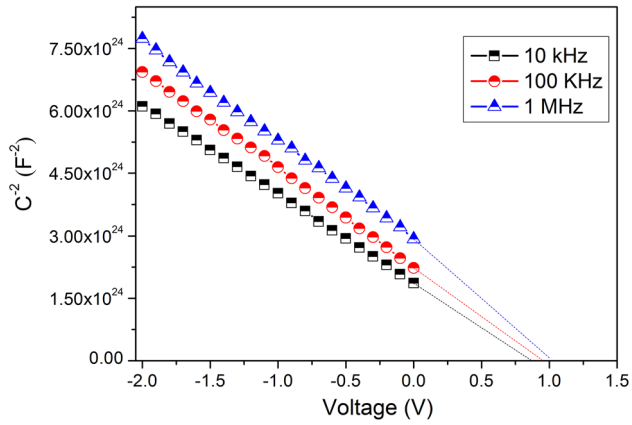

Fig. 4. Reverse-bias C^{-2} versus *V* plots of typical TMAH-treated Ni/Au/Al_2O_3/GaN MIS diode at different frequencies at room temperature.

response to this signal. The interface state capacitance appears directly in parallel with the depletion capacitance, resulting in higher total capacitance at low frequencies. The capacitance is low at high frequencies since the interface state charges do not contribute to the diode capacitance. To confirm the Ni/Au/Al_2O_3/GaN MIS structure, it was investigated using MOS *C–V* measurements (at 1 MHz), as shown in the inset of Fig. 3. A small, injection-type hysteresis loop is seen for the Ni/Au/GaN and Ni/Au/Al_2O_3/GaN MIS diodes. However, it is observed that the hysteresis loop is wider for the Ni/Au/Al_2O_3/GaN MIS diode after insertion of the insulating layer (Al_2O_3), confirming the MIS structure behavior, as well as the reduction in the interface state density at the oxide–semiconductor junction. Similar results were observed for Au/SiO_2/GaN MIS structures.[28] The capacitance of a Schottky diode per unit area under reverse bias (V_R) is given by the depletion capacitance[22,23]

$$C = \left[\left(\frac{q\varepsilon_S N_D A^2}{2}\right)\left(V_{bi} - \frac{k_B T}{q} - V_R\right)\right]^{1/2}, \quad (5)$$

where ε_S is the permittivity of the semiconductor ($\varepsilon_S = 9.5\varepsilon_0$) and N_D is the doping density. Figure 4 shows a plot of $1/C^2$ as a function of bias voltage *V* at different frequencies at 300 K for the TMAH-treated Ni/Au/Al_2O_3/GaN MIS diode. The *x*-intercept of the plot of $1/C^2$ versus V_R is V_0, being related to the built-in potential V_{bi} by the equation $V_{bi} = V_0 + kT/q$, where *T* is absolute temperature. The barrier height is given by $\varphi_{bo}^{CV} = V_{bi} + V_n$, where $V_n = (kT/q)\ln(N_C/N_D)$. The SBH was estimated from the *C–V* results at room temperature, yielding values of 1.04 eV, 1.1 eV, and 1.16 eV at frequency of 10 kHz, 100 kHz, and 1 MHz, respectively. The SBH obtained from the *C–V* characteristics (f = 1 MHz) at 300 K is higher than that obtained from the *I–V* characteristics at 300 K. The *C–V* method averages over the entire area and measures the Schottky barrier diode, whereas the barrier height obtained by the *I–V* method includes any barrier-lowering effect due to the interfacial oxide layer or the interface states, yielding an effective barrier height. However, the difference between the barrier heights obtained from the *C–V* characteristics (f = 1 MHz) or *I–V* characteristics at 300 K is small. This shows that the Schottky contacts are expected to be homogeneous, as also confirmed by the near-unity ideality factor of the TMAH-treated Ni/Au/Al_2O_3/GaN MIS diode obtained from *I–V* characteristics at 300 K.

To determine the origin of interface states in equilibrium with the semiconductor, an ideality factor greater than one was proposed by Card and Rhoderick[29] in the form $n(V) = 1 + \delta/\varepsilon_i[\varepsilon_S/W_d + N_{SS}]$. The energy density distribution of interface states (N_{SS}) in equilibrium with the semiconductor can be evaluated from measured *C–V* and *I–V* data using

$$N_{SS} = \frac{1}{q}\left[\frac{\varepsilon_i}{\delta}\left((n(V) - 1) - \frac{\varepsilon_S}{W_d}\right)\right], \quad (6)$$

where W_d is the depletion layer width and δ is the thickness of the insulator (Al_2O_3). The value of ε_i for the Al_2O_3 layer is $9.8\varepsilon_0$. The voltage dependence of the effective barrier height ϕ_e is given by the relations

$$\varphi_e = \varphi_b + \beta V \quad (7)$$

and

$$\frac{d\varphi_e}{dV} = \beta = 1 - \frac{1}{n(V)}. \quad (8)$$

The energy distribution of interface states (E_{SS}) with respect to the bottom of the conduction band is given by

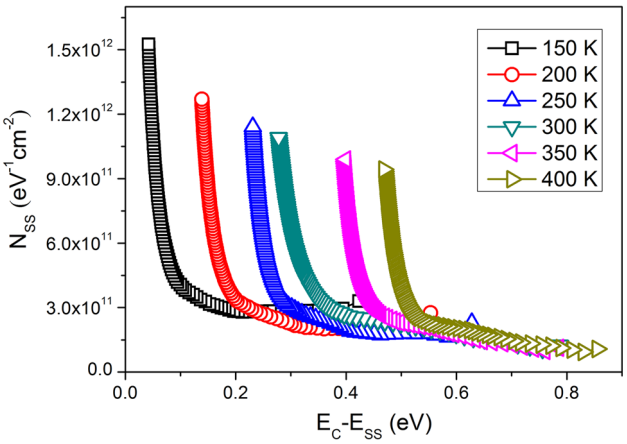

Fig. 5. Interface state density, N_{SS}, as function of $E_C - E_{SS}$ for TMAH-treated Ni/Au/Al_2O_3/GaN MIS diode at different temperatures.

$$E_C - E_{SS} = q(\varphi_e - V). \quad (9)$$

Substituting the voltage dependence $n(V)$, δ, and W_d into Eq. 6 yields N_{SS} as a function of $(E_C - E_{SS})$, as shown in Fig. 5. The N_{SS} value for the TMAH-treated Ni/Au/Al_2O_3/GaN MIS diode decreases with increasing $E_C - E_{SS}$ as a function of temperature. Moreover, the exponential growth of N_{SS} toward the top of the valence band is noticeable. The magnitude of N_{SS}, as determined by Terman's method[30] at 150 K, varied from 1.52×10^{12} eV^{-1} cm^{-2} ($E_C - 0.042$ eV) to 3.29×10^{11} eV^{-1} cm^{-2} ($E_C - 0.43$ eV), whereas the magnitude of the interface state density at 400 K varied from 9.42×10^{11} eV^{-1} cm^{-2} ($E_C - 0.47$ eV) to 1.07×10^{11} eV^{-1} cm^{-2} ($E_C - 0.86$ eV). The interface state density in equilibrium with the semiconductor increases with the ideality factor over the range from 1 to 2, indicating that larger ideality factors correspond to higher interface state densities.[29] Generally, interface trap charges are located at the insulator–semiconductor interface, with energy states in the semiconductor forbidden bandgap. Consequently, the behavior of the forward-bias *I–V* characteristics deviates from ideal, being precisely controlled by the interface states. The decrease in the interface state density at TMAH-treated GaN surfaces is mainly due to the decrease in deep electronic states and removal of recess-induced protrusions on the GaN surface.[20,21] As a result, the deep electronic states nonuniformly distributed in the GaN bandgap are directly proportional to temperature. In addition, N_{SS} decreases with increasing temperature, maybe due to molecular restructuring and reordering of the metal–semiconductor interface under the effect of temperature.[31]

The characteristic energy E_{00}, which is related to the carrier transmission probability through the barrier, is given by $E_{00} = h/4\pi\sqrt{N_D/m^*\varepsilon_S}$,[22,23,32]

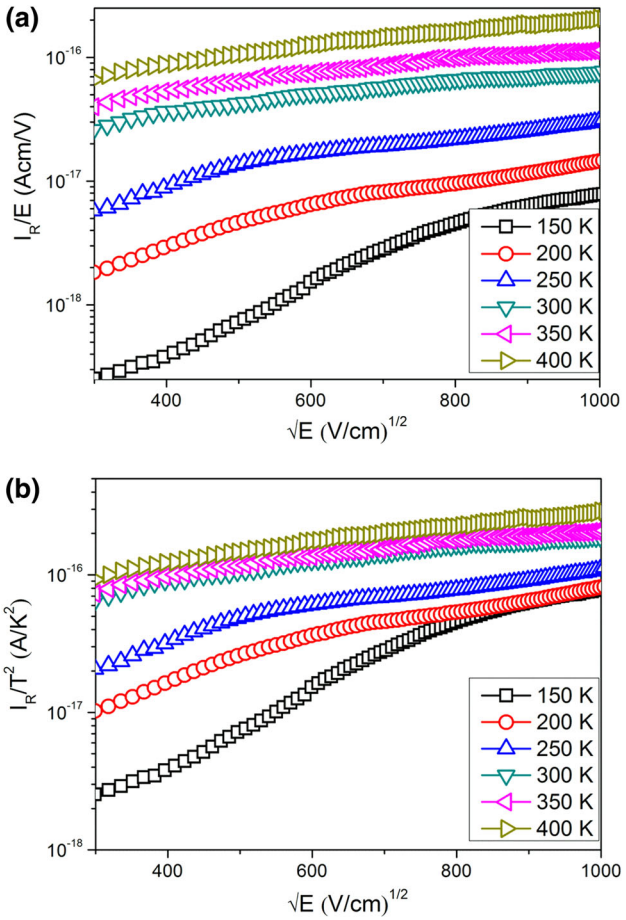

Fig. 6. (a) I_R/E versus $E^{1/2}$ for PFE mechanism and (b) I_R/T^2 versus $E^{1/2}$ for SE mechanism of TMAH-treated Ni/Au/Al_2O_3/GaN MIS diodes in reverse-bias region.

where h is Planck's constant and N_D is the doping concentration. Its value is 4.03×10^{16} cm^{-3} as estimated using the *C–V* technique. It is worth noting that tunneling becomes important when $E_{00} \rangle\rangle kT$ while thermionic field emission (TFE) becomes important if $E_{00} \approx kT$. The value of E_{00} is found to be 1.26 meV at 300 K. According to the transport mechanism, $E_{00} \langle\langle kT$ (where kT is the thermal energy, being 25.8 meV at 300 K), so TE is the dominant current theory at 300 K.

Figure 1 reveals that the reverse-bias current is not saturated, but increases with increasing bias. Usually, carrier recombination in the depletion layer and image-force lowering of the barrier height tend to increase the ideality factor and often dominate the reverse characteristics of Schottky diodes because the reverse bias increases the electric field in the junction. As the current transport mechanism dominating the reverse leakage current (I_R) of the TMAH-treated Ni/Au/Al_2O_3/GaN MIS diodes, the Poole–Frenkel emission (PFE) and Schottky emission (SE) models are considered.[32–34] The plots of $\ln(I_R/E)$ and $\ln(I_R/T^2)$ versus $(E)^{1/2}$ are shown in Fig. 6a and b, while the PFE and SE

transport mechanisms are illustrated schematically in Fig. 7. The PFE current is generally described as $I_R \propto E\exp\left(1/k_BT\sqrt{qE/\pi\varepsilon}\right)$ and the contribution to I_R by Schottky lowering is given as $I_R \propto T^2\exp\left(1/2k_BT\sqrt{qE/\pi\varepsilon}\right)$, where E is the maximum electric field in the junction.[32,33,35] The slope of linear curves on PFE and SE plots can be found as[32–34]

$$S = \frac{q}{nkT}\left(\frac{q}{\pi\varepsilon}\right)^{1/2}, \qquad (10)$$

where n = 1 for PFE and n = 2 for SE. Based on the values in Table II, the slope determined by fitting to the I–V curves at 150 K, 200 K, and 250 K is almost equal to the theoretical PFE value. The results of this analysis are therefore consistent with the PFE mechanism, and the primary field-enhanced carrier transport for the reverse junction at 150 K, 200 K, and 250 K is dominated by PFE with a donor-like trap and thermal carrier detrapping from the bulk oxide into the conduction band (Fig. 7a). Therefore, this is a bulk-limited conduction process.[22,23] In this mechanism, conduction occurs due to defect states and a very small amount of carriers follow the over barrier. Moreover, experimental data in the high-temperature (300 K to 400 K) region are consistent with SE (Fig. 7b), where carriers absorb thermal energy and are then emitted over the potential barrier at the interface,[36] while a few carriers follow through the interface barrier. Both PFE and SE are associated with barrier lowering in the presence of an external electric field; in both cases, electron emission requires thermal excitation. SE takes place at the dielectric interface, whereas PFE takes place through traps in the bulk of the dielectric. The origin of these traps in this case has been widely reported by several authors to be donor-like traps within the ALD Al_2O_3 layer, most likely oxygen vacancies.[37,38] In fact, energy levels of oxygen vacancies lie approximately 3.12 eV to 3.98 eV above the valance-band edge of Al_2O_3, in approximate alignment with the valance-band maximum of GaN at the interface, considering the ~2.2 eV conduction-band offset between Al_2O_3 and GaN.[37] Previous studies predicted PFE trap-assisted tunneling, with Fowler–Nordheim direct tunneling at higher voltages in the forward-bias direction.[20] The present results for the temperature and field dependence of the current demonstrate a transition in the dependence of the reverse junction current from PFE to SE at temperature of 150 K to 400 K.

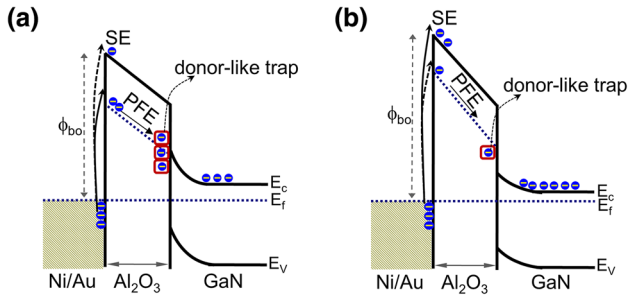

Fig. 7. Schematic energy band diagrams of TMAH-treated Ni/Au/Al_2O_3/GaN MIS diode for (a) <300 K and (b) ≥300 K. Donor-like traps (*red symbol*) at the interface dominate below room temperature, resulting in the PFE mechanism, while traps are decreased by absorption of thermal energy by carriers at and above room temperature, leading to the SE mechanism.

CONCLUSIONS

The temperature-dependent electrical properties and carrier transport mechanisms of TMAH-treated Al_2O_3/GaN MIS diodes were investigated. The results reveal that the barrier height (I–V) increased while the ideality factor decreased with increase in temperature. The series resistance (R_S) and interface state density (N_{SS}) of the TMAH-treated Al_2O_3/GaN MIS diode were found to decrease with temperature from 150 K to 400 K. Moreover, the carrier transport mechanism was investigated at various electric fields and temperatures, revealing essentially different mechanisms. Based on the experimental results, it is suggested that the mechanism for the TMAH-treated Al_2O_3/GaN MIS diode is PFE at 150 K to 250 K, whereas SE dominates the carrier transport mechanism at elevated temperatures (≥300 K). These distinct mechanisms could be due to the effect of different carrier transport in the TMAH-treated Al_2O_3/GaN MIS diode with, e.g., SE taking place at the dielectric interface whereas PFE occurs through traps in the bulk of the dielectric.

Table II. Calculated and experimental slopes for PFE and SE mechanisms

Temperature (K)	PFE [(V/cm)$^{-1/2}$]		SE [(V/cm)$^{-1/2}$]	
	Calculated	From fit	Calculated	From fit
150	0.0191	0.0187	0.0096	0.0151
200	0.0142	0.0139	0.0071	0.0119
250	0.0115	0.0112	0.0058	0.0089
300	0.0095	0.0068	0.0048	0.0047
350	0.0082	0.0042	0.0041	0.0043
400	0.0072	0.0021	0.0036	0.0035

ACKNOWLEDGEMENT

This work was partially supported by the New and Renewable Energy Core Technology Program of the Korea Institute of Energy Technology Evaluation and Planning (KETEP) granted financial resource from the Ministry of Trade, Industry, and Energy, Republic of Korea (No. 20143030011950).

REFERENCES

1. M.S.P. Reddy, H. Park, S.-M. Kim, S.-H. Jang, and J.-S. Jang, *J. Mater. Chem. C* 3, 8873 (2015).
2. D. Zhu, D.J. Wallis, and C.J. Humphreys, *Rep. Prog. Phys.* 76, 106501 (2013).
3. M.S.P. Reddy, B.-J. Kim, and J.-S. Jang, *Opt. Express* 22, 908 (2014).
4. H.-S. Kang, M.S.P. Reddy, D.-S. Kim, K.-W. Kim, J.-B. Ha, Y.-S. Lee, H.-C. Choi, and J.-H. Lee, *J. Phys. D Appl. Phys.* 46, 155101 (2013).
5. S. Strite and H. Morkoc, *J. Vac. Sci. Technol. B.* 10, 1237 (1992).
6. Y.Q. Wu, T. Shen, P.D. Ye, and G.D. Wilk, *Appl. Phys. Lett.* 90, 143504 (2007).
7. A. Christou and F. Fantini, *IEEE Trans. Device Mater. Reliab.* 8, 239 (2008).
8. M. Tapajna and J. Kuzmik, *Appl. Phys. Lett.* 100, 113509 (2012).
9. T.-H. Tsai, H.-I. Chen, K.-W. Lin, Y.-W. Kuo, C.-F. Chang, C.-W. Hung, L.-Y. Chen, T.-P. Chen, Y.-C. Liu, and W.-C. Liu, *Sens. Actuators B* 136, 338 (2009).
10. F. Tian and E.F. Chor, *Phys. Status Solidi C* 5, 1953 (2008).
11. M.S.P. Reddy, A.A. Kumar, and V.R. Reddy, *Thin Solid Films* 519, 3844 (2011).
12. T.-C. Lee and J.-T. Yan, *Sens. Actuators B* 147, 723 (2010).
13. B.P. Lakshmi, M.S.P. Reddy, A.A. Kumar, and V.R. Reddy, *Curr. Appl. Phys.* 12, 765 (2012).
14. L.X. Yang, Z. Kai, Z. Chang, Z.X. Feng, E.Y. Fei, L. Ping, and H. Yue, *Chin. Phys. B* 23, 057301 (2014).
15. A. Shetty, B. Roul, S. Mukundan, L. Mohan, G. Chandan, K.J. Vinoy, and S.B. Krupanidhi, *AIP Adv.* 5, 097103 (2015).
16. K.-Y. Park, H.-I. Cho, J.-H. Lee, S.-B. Bae, C.-M. Jeon, J.-L. Lee, D.-Y. Kim, C.-S. Lee, and J.-H. Lee, *Phys. Status Solidi C* 2351 (2003).
17. P.D. Ye, B. Yang, K.K. Ng, J. Bude, G.D. Wilk, S. Halder, and J.C.M. Hwang, *Appl. Phys. Lett.* 86, 063501 (2005).
18. Z.H. Liu, G.I. Ng, S. Arulkumaran, Y.K.T. Maung, K.L. Teo, S.C. Foo, and V. Sahmuganatham, *Appl. Phys. Lett.* 95, 223501 (2009).
19. Z. Yang, R. Wang, D. Wang, B. Zhang, K.M. Lau, and K.J. Chen, *Sens. Actuators A* 130, 371 (2006).
20. K.-W. Kim, S.-D. Jung, D.-S. Kim, H.-S. Kang, K.-S. Im, J.-J. Oh, J.-B. Ha, J.-K. Shin, and J.-H. Lee, *IEEE Electron Device Lett.* 32, 1376 (2011).
21. M.S.P. Reddy, J.-H. Lee, and J.-S. Jang, *Electron. Mater. Lett.* 2, 411 (2014).
22. E.H. Rhoderick and R.H. Williams, *Metal-Semiconductor Contacts*, 2nd ed. (Clarendon Press, Oxford, 1988).
23. M. Sze, *Physics of Semiconductor Devices*, 2nd ed. (New York: Wiley, 1969).
24. M.S.P. Reddy, H.-S. Kang, J.-H. Lee, V.R. Reddy, and J.-S. Jang, *J. Appl. Polym. Sci.* 131, 39773 (2014).
25. R.T. Tung, *Phys. Rev. B* 45, 13509 (1992).
26. H. Cetin, B. Sahin, E. Ayylidiz, and A. Turut, *Phys. B* 364, 133 (2005).
27. S.K. Cheung and N.W. Cheung, *Appl. Phys. Lett.* 49, 85 (1986).
28. V.R. Reddy, M.S.P. Reddy, B.P. Lakshmi, and A.A. Kumar, *J. Alloys Compd.* 509, 8001 (2011).
29. H.C. Card and E.H. Rhoderick, *J. Phys. D Appl. Phys.* 4, 1589 (1971).
30. L.M. Terman, *Solid-State Electron.* 5, 285 (1962).
31. B. Akkal, Z. Benemara, A. Boudissa, N.B. Bouiadjra, M. Amrani, and I. Bideux, *Mater. Sci. Eng. B* 55, 162 (1998).
32. V. Janardhanam, H.-K. Lee, K.-H. Shim, H.-B. Hong, S.-H. Lee, K.-S. Ahn, and C.-J. Choi, *J. Alloys Compd.* 504, 146 (2010).
33. V.R. Reddy, *Appl. Phys. A* 122, 519 (2016).
34. H.D. Lee, *IEEE Trans. Electron Devices* 47, 762 (2000).
35. A. Chatterjee, M. Rodder, and I.C. Chen, *IEEE Trans. Electron Devices* 45, 1246 (1998).
36. J. Lin, S. Banerjee, J. Lee, and C. Teng, *IEEE Electron Device Lett.* 11, 191 (1990).
37. J.R. Weber, A. Janotti, and C.G. Van de Walle. *J. Appl. Phys.* 109, 033715 (2011).
38. E.J. Kim, L. Wang, P.M. Asbeck, K.C. Saraswat, and P.C. Mclntyre, *Appl. Phys. Lett.* 96, 012906 (2010).